

# AEROELASTIC ANALYSIS OF BEARINGLESS ROTORS WITH COMPOSITE FLEXBEAM IN HOVER AND FORWARD FLIGHT

Lim, In-Gyu\* and Lee, In\*\*

\* Graduate research assistant, \*\* Professor

Department of Aerospace Engineering, KAIST, Daejeon 305-701, Korea.

**Keywords:** *Bearingless rotors, Composite material, Flexbeam and Aeroelasticity.*

## Abstract

*The aeroelastic response and stability of bearingless rotors are investigated using large deflection beam theory in hover and forward flight. The bearingless configuration consists of a single flexbeam with a wrap-around type torque tube and pitch links located at the leading edge and trailing edge of the torque tube. The outboard main blade, flexbeam, and torque tube are all assumed to be an elastic beam undergoing arbitrary large displacements and rotations, which are discretized into beam finite elements. For the analysis of composite bearingless rotors, flexbeam is assumed to be rectangular section made of laminate. The sectional elastic constants of a composite flexbeam including warping deformations are determined from the refined cross-sectional finite element method. Numerical results of the static deflections and the aeroelastic modal damping are presented for various configurations of composite flexbeam.*

## 1 Introduction

Structural dynamic and aeroelastic modeling of composite blades undergoing moderate or large deflections and their application to the study of hingeless, bearingless, and tilt-rotor blade aeroelasticity as well as coupled rotor-fuselage problems has been a particularly active area of research[1]. In recent years there has been growing interest in bearingless rotor because of design simplicity, more control power and maintenance. A bearingless rotor is one example of a hingeless rotor in which the pitch bearing, flap and lag hinges are eliminated. The bearingless configuration shown in Fig. 1 consists of a single flexbeam with a wrap-around type torque tube, the pitch links located at the leading edge and trailing edge of the torque tube

and main blade. The distinguishing feature of the bearingless rotor is both torsionally soft flexbeam and torsionally stiff torque tube. The aeroelastic stability of a rotor blade is inherently a nonlinear phenomenon. The analysis of a bearingless rotor blade is more involved than that of a hingeless rotor blade because of the redundancy of load paths at the root and nonlinear bending-torsion coupling effects. Most modern helicopter rotor blades are built of composite materials because they have better fatigue life and damage tolerance than metal blades. The increased use of composite materials in blade design also provides the potential for aeroelastic tailoring. Generally, studies on rotor blades have been performed for global deformation and cross-sectional analyses. One-dimensional global deformation analyses of rotor blades considering the geometrical nonlinearity have been classified into two-type beam theories of a moderate deflection-type and a large deflection-type. It is also important to obtain accurate effective sectional stiffness through the cross-sectional analysis with one-dimensional global deformation analysis. The cross-sectional analysis has been carried out using both direct analytical methods and finite element methods. Finite element methods give more accurate results than the analytical methods because it is difficult to obtain exact sectional stiffness of composite beams. Most of the structural dynamic models for rotor blades are based on moderate deflection type beam theories. These theories are based on ordering schemes and are valid for moderate deflections[2]. In the literature, some attempts to analyze the stability of bearingless rotors using the moderate deflection type beam theory have been reported in hover[3,4] and forward flight[5,6]. A general purpose analysis, however, demands a large deflection model without any artificial restrictions on displacements or rotations due to the deformation

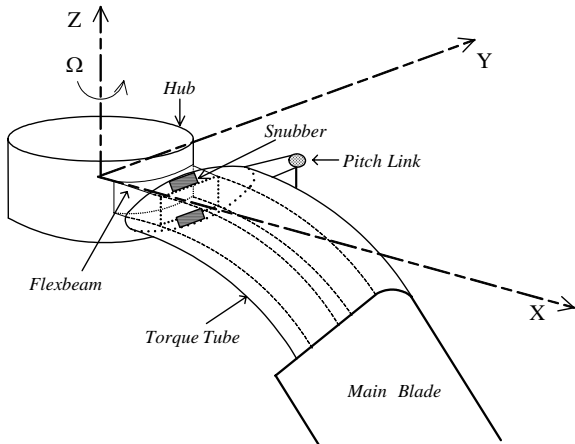


Fig. 1. Bearingless rotor blade configuration

and the degree of nonlinearity. The ordering scheme, although a valuable tool in special purpose research, is not desirable in a general purpose approach. To overcome the limitations of previous models, structural models that are valid for large deflection and are not based on ordering schemes have been developed and used for static and dynamic[7-10] analyses of composite beams. The only restriction on the deformation in these theories is that the strain is relatively small compared with unity. There are no small angle approximations made, and all kinematic nonlinear effects are included in the formulation. To date, there have been relatively few studies on aeroelastic analysis of rotor blades using large deflection-type beam theories, and this type of beam theory has almost been applied to hingeless rotor blades[11,12].

In the present study the aeroelastic stability analysis of isotropic and composite bearingless rotors is investigated using a large deflection beam theory in hover and forward flight. Two-dimensional quasi-steady strip theory is used for aerodynamic computation in hover and forward flight. The composite flexbeam is idealized as a laminated rectangular beam and effective elastic constants are obtained from the cross-sectional finite element method. Nonlinear, periodic blade steady response solutions are obtained using a time finite element method on full finite element equation in forward flight condition. Blade response analysis is fully coupled with vehicle trim analysis to obtain nonlinear blade response, pilot controls, and vehicle attitude. The aeroelastic response is calculated by a time-marching solution procedure from the linearized stability equation about the nonlinear equilibrium position, and then the stability analysis is performed by using a moving block analysis. Numerical results are calculated for selected

bearingless blade configurations based on the lay-up of laminae in the flexbeam.

## 2 Analysis

### 2.1 Kinematics

Consider the rotor blade rotating with angular velocity  $\Omega$  depicted in Fig. 2. Here the triad  $\mathbf{I}_1$ ,  $\mathbf{I}_2$  and  $\mathbf{I}_3$  is fixed in an inertia frame, the triad  $\mathbf{i}_1$ ,  $\mathbf{i}_2$  and  $\mathbf{i}_3$  fixed in a reference frame which rotates with respect to the inertia frame at a constant angular velocity  $\Omega\mathbf{I}_3$ , the triad  $\mathbf{e}_1$ ,  $\mathbf{e}_2$  and  $\mathbf{e}_3$  attached to a reference line along the axis of the undeformed blade, and the triad  $\mathbf{e}_1^*$ ,  $\mathbf{e}_2^*$  and  $\mathbf{e}_3^*$  attached to a reference line along the axis of the deformed blade. The geometrical nonlinearities are described using coordinate transformation matrices with the Euler angles in the present large deflection-type beam theory.

$$\mathbf{e}_i^* = \mathbf{t}_e(x_1)\mathbf{e}_i = \mathbf{T}(x_1)\mathbf{i}_i, \mathbf{T}(x_1) = \mathbf{t}_e(x_1)\mathbf{t}_g(x_1) \quad (1)$$

The transformation matrices  $\mathbf{t}_g$ ,  $\mathbf{t}_e$ , and  $\mathbf{T}$  are functions of the curvilinear axial coordinate  $x_1$ . Assuming that initial curvatures are small and shearing strains are much smaller than unity in the Green-Lagrangian strain components, strain-displacement relations can be expressed as follows :[10]

$$\begin{aligned} \varepsilon_{11} &= \bar{\varepsilon}_{11} + x_3\kappa_2 - x_2\kappa_3 + w_1' & \varepsilon_{22} &= w_{2,2} \\ \gamma_{12} &= 2\bar{\varepsilon}_{12} - x_3\kappa_1 + w_{1,2} + w_2' & \gamma_{23} &= w_{2,3} + w_{3,2} \\ \gamma_{13} &= 2\bar{\varepsilon}_{13} + x_2\kappa_1 + w_{1,3} + w_3' & \varepsilon_{33} &= w_{3,3} \end{aligned} \quad (2)$$

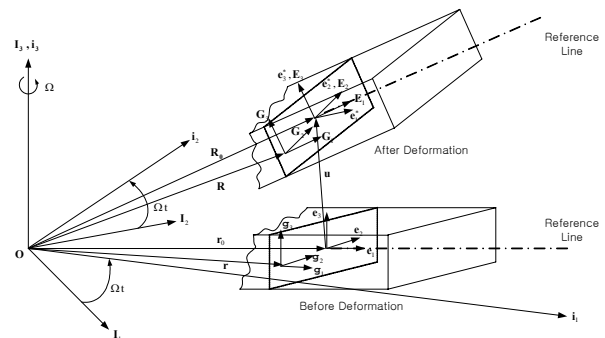


Fig. 2. Geometry and coordinate systems of a rotor blade before and after deformation

where  $x_1$ ,  $x_2$  and  $x_3$  are curvilinear coordinates and  $w_1$ ,  $w_2$  and  $w_3$  are the general warping displacements of an arbitrary point on the cross section. The

force strains  $(\bar{e}_{11}, 2\bar{e}_{12}, 2\bar{e}_{13})$  and moment strains  $(\kappa_1, \kappa_2, \kappa_3)$  components are given in Ref. [10]. Here,  $(\cdot)'$  means the derivative with respect to  $x_1$  and  $(\cdot)_i$  means the derivatives with respect to  $x_i$ ,  $i = 2, 3$ .

## 2.2 Cross-sectional analysis

Considering an energy equilibrium in an infinitesimal slice of a loaded beam, the following governing equations for the cross-sectional analysis can be obtained :[8]

$$\{\mathbf{Q}'\} + \begin{bmatrix} \tilde{\kappa} & 0 \\ \tilde{\Omega}_2 + \tilde{e} & \tilde{\kappa} \end{bmatrix} \{\mathbf{Q}\} + \begin{Bmatrix} \mathbf{f} \\ \mathbf{m} \end{Bmatrix} = 0 \quad (3)$$

$$[\mathbf{M}]\{\mathbf{W}''\} - [\mathbf{H}]\{\mathbf{W}'\} - [\mathbf{E}]\{\mathbf{W}\} + [\mathbf{L}]\{\Psi'\} - [\mathbf{R}]\{\Psi\} = 0$$

$$[\mathbf{L}]^T\{\mathbf{W}'\} + [\mathbf{R}]^T\{\mathbf{W}\} + [\mathbf{A}]\{\Psi\} = \{\mathbf{Q}\}$$

In the present work, the cross-sectional modeling for the rectangular flexbeam is proposed as Fig. 3. The displacement in the thickness direction is Interpolated as a linear function and integrated analytically. In the other direction, a cubic Lagrangian function was used and integrated using Gauss-Legendre quadrature. If  $\mathbf{f}$  and  $\mathbf{m}$  are taken to be zero in Eq. (3). In unloaded condition, we can obtain effective elastic sectional constants.

$$\begin{Bmatrix} \mathbf{F} \\ \mathbf{M} \end{Bmatrix} = \begin{bmatrix} \mathbf{A} & \mathbf{B} \\ \mathbf{B}^T & \mathbf{D} \end{bmatrix} \begin{Bmatrix} \bar{\mathbf{e}} \\ \bar{\boldsymbol{\kappa}} \end{Bmatrix} \quad (4)$$

where  $\mathbf{F}$  and  $\mathbf{M}$  are the cross-sectional force and moment stress vectors in the deformed beam basis, and  $\bar{\mathbf{e}}$  and  $\bar{\boldsymbol{\kappa}}$  vectors are defined as follows :  $\bar{\mathbf{e}} = \{\bar{e}_{11} \ 2\bar{e}_{12} \ 2\bar{e}_{13}\}^T$ ,  $\bar{\boldsymbol{\kappa}} = \{\kappa_1 \ \kappa_2 \ \kappa_3\}^T$ . The matrices  $\mathbf{A}$ ,  $\mathbf{B}$  and  $\mathbf{D}$  are  $3 \times 3$  matrices that depend on the material properties and the geometry of the cross section. In the case of isotropic material, these matrices are represented by the diagonal term.

## 2.3 Global analysis and finite element equation

The outboard main blade, flexbeam, torque tube are all assumed to be an elastic beam. The equations of motion for a bearingless rotor blade are obtained using Hamilton's principle :

$$\int_{t_1}^{t_2} \sum_{i=1}^m (\delta U_i - \delta T_i - \delta W_i) dt = 0 \quad (5)$$

where  $\delta U_i$ ,  $\delta T_i$  and  $\delta W_i$  are the variation of strain energy, the variation of kinetic energy and the virtual work of applied force about flexbeam, torque tube and main blade, respectively.

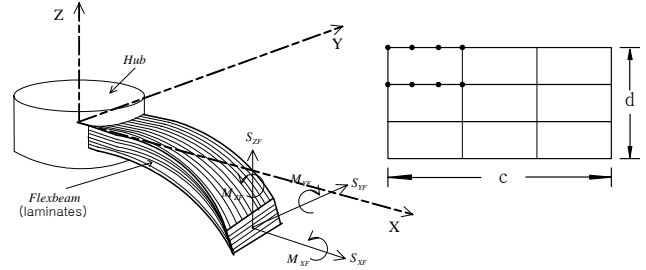


Fig. 3. Composite flexbeam cross section and sectional nodal distribution

Pitch control to the main blade is applied through a torsionally stiff torque tube by rotating it with pitch link, which in turn twists the flexbeam. A pitch link is connected to the root end of the torque tube at its leading or trailing edge. The pitch links model is replaced by spring stiffness. In the global finite element energy expression, the spring contributes an additional strain energy term. When a pitch link is connected at torque tube's leading edge, the added strain energy is :

$$U_p = \frac{1}{2} K_p (w_i + \theta_i d)^2 \quad (6)$$

where  $K_p$  is the pitch link stiffness,  $d$  is pitch link offset from elastic axis,  $w_i$  and  $\theta_i$  are elastic flap and torsion displacements, respectively.

In hover, the induced velocity  $v_{id}$  is taken to be steady and uniform along the blade radius and is set equal to the value of inflow given by the combined momentum and blade element theory at a radial station  $r = 0.75R$ . A linear inflow model is used for the rotor inflow distribution in forward flight. In hover, the nonlinear finite element equations of motion in matrix form can be formulated as:

$$\begin{aligned} & [\mathbf{M}(\mathbf{q}) - \mathbf{M}_A(\mathbf{q})]\{\ddot{\mathbf{q}}\} + [\mathbf{G}(\mathbf{q}) - \mathbf{C}_A(\mathbf{q})]\{\dot{\mathbf{q}}\} \\ & + \mathbf{P}(\mathbf{q}) - \mathbf{P}_C(\mathbf{q}) = \mathbf{P}_A(\mathbf{q}) \end{aligned} \quad (7)$$

where  $[\mathbf{M}]$ ,  $[\mathbf{M}_A]$ ,  $[\mathbf{G}]$ , and  $[\mathbf{C}_A]$  are the mass, aerodynamic apparent mass, gyroscopic damping, and aerodynamic damping matrices in finite elements, respectively. The term  $\mathbf{P}$  is the internal elastic force vector,  $\mathbf{P}_C$  is the centrifugal load vector, and  $\mathbf{P}_A$  is the steady aerodynamic load vector. To

solve the governing equation of motion (7), dropping all time dependent terms, the nonlinear steady-state deformation is calculated through the iterative Newton-Raphson method. In forward flight, the nonlinear, periodic steady response is obtained using a time finite element technique. The virtual energy expression for the Hamilton's weak form can be obtained as follows :

$$\int_{\psi_i}^{\psi_f} \delta \mathbf{y}^T \mathbf{l} d\psi = \delta \mathbf{y}^T \mathbf{b} \Big|_{\psi_i}^{\psi_f} \quad (8)$$

$$\delta \mathbf{y} = \begin{Bmatrix} \delta \dot{\mathbf{q}} \\ \delta \mathbf{q} \end{Bmatrix} \quad \mathbf{l} = \begin{Bmatrix} \mathbf{L}_{\dot{\mathbf{q}}} \\ \mathbf{L}_{\mathbf{q}} + \mathbf{Q} \end{Bmatrix} \quad \mathbf{b} = \begin{Bmatrix} \mathbf{0} \\ \mathbf{p} \end{Bmatrix}$$

where  $\mathbf{Q}$  is the generalized forces and  $\mathbf{L}$  is the Lagrangian of the system.  $\mathbf{L}_{\dot{\mathbf{q}}}$  and  $\mathbf{L}_{\mathbf{q}}$  are the partial derivatives of  $\mathbf{L}$  with respect to generalized coordinates  $\dot{\mathbf{q}}$  and  $\mathbf{q}$ , respectively, which are composed of displacements and Euler angles, while  $\mathbf{p} = \mathbf{L}_{\dot{\mathbf{q}}}$  is the column vector of the generalized moment.  $\psi_i$  and  $\psi_f$  represent the initial and final states of non-dimensionalized time, respectively. Using a first order Taylor series expansion of the left-hand side of Eq.(8) with respect to a given state vector  $\bar{\mathbf{y}}$ , the following governing equation can be derived in an incremental form :

$$\int_{\psi_i}^{\psi_f} \delta \mathbf{y}^T \bar{\mathbf{l}} d\psi + \int_{\psi_i}^{\psi_f} \delta \mathbf{y}^T \bar{\mathbf{K}} \Delta \mathbf{y} d\psi = \delta \mathbf{y}^T \mathbf{b} \Big|_{\psi_i}^{\psi_f} \quad (9)$$

$$\bar{\mathbf{K}} = \begin{bmatrix} \mathbf{L}_{\dot{\mathbf{q}}\dot{\mathbf{q}}} & \mathbf{L}_{\dot{\mathbf{q}}\mathbf{q}} \\ \mathbf{L}_{\mathbf{q}\dot{\mathbf{q}}} + \mathbf{Q}_{\dot{\mathbf{q}}} & \mathbf{L}_{\mathbf{q}\mathbf{q}} + \mathbf{Q}_{\mathbf{q}} \end{bmatrix}$$

For the stability analysis in hover, it is assumed that the flutter motion is a small perturbation about the equilibrium position, and the linearized flutter equations are then transformed to the modal space. The transformed modal equations are solved through the p-k modal flutter analysis. In forward flight, the blade perturbation equations of motion are also linearized about the equilibrium position. The initial value of the perturbed blade motion is taken to be 10% of the equilibrium position. From the initial perturbation, the blade is set free to move and the blade perturbation equations of motion are integrated by the fourth-order Runge-Kutta method. After the time histories of the blade lag, flap, and torsional deflections are known, the modal damping

and frequency of any desired mode can be determined from the moving block analysis.

### 3 Numerical Results and Discussion

The sectional elastic constants of composite flexbeam are obtained in unloaded condition using the refined cross-sectional finite element method. Then, these sectional elastic constants are used for the one-dimensional global analysis. For calculating the elastic constants, nine elements about rectangular section are used in cross-sectional analysis. For the global deformation analysis, the blade is discretized into seven four-noded cubic elements; three elements for the main blade, two elements for the flexbeam and two elements for the torque tube. For results, only the

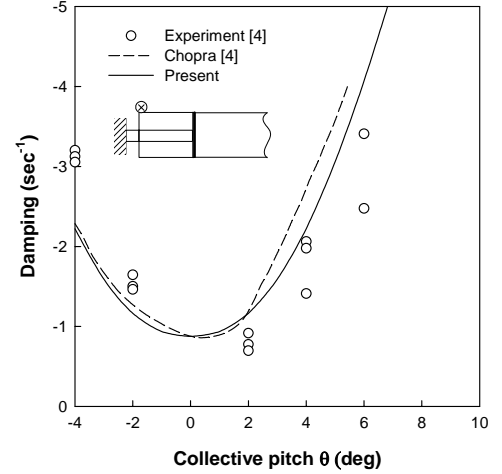


Fig. 4. Lag damping as a function of collective pitch (leading edge pitch links)

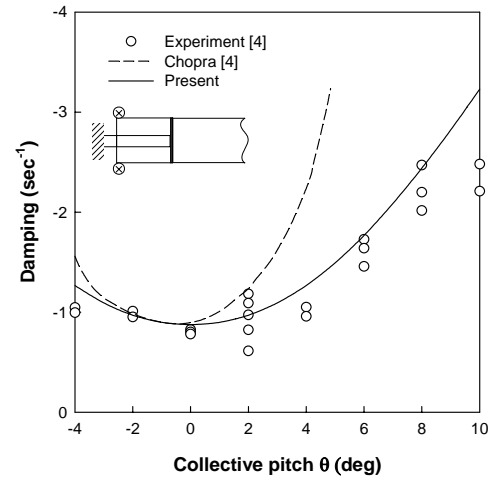


Fig. 5. Lag damping as a function of collective pitch (both edge pitch links)

flexbeam is modeled as a laminated beam; the main blade and the torque tube are treated as made of metals (isotropic). The time period of one rotor revolution is discretized into six four-noded cubic elements in time domain for reasonably good convergence. The static analyses of the composite rectangular beam based on this method are validated. Aeroelastic analyses of bearingless rotors with composite flexbeam are performed using the large deflection-type beam theory in hover and forward flight condition. To verify the validity and accuracy of the present approach, figs. 4 and 5 show the results of the present aeroelastic stability analysis of isotropic bearingless rotors in hover compared with the existing solutions given in [4]. The present results are relatively better correlated with the experimental data than the analysis results in [4] at all collective pitch angles.

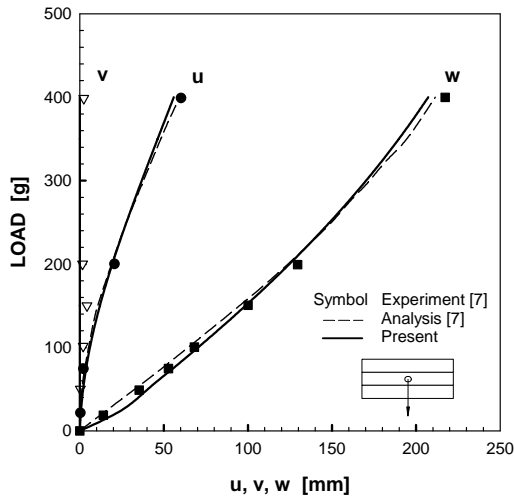


Fig. 6. Displacements for a  $[0/90]_{3S}$  beam

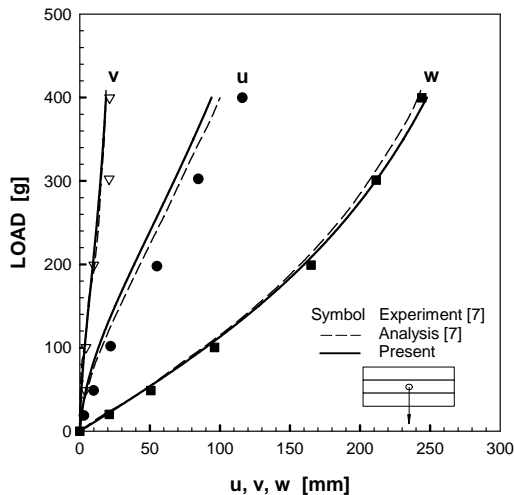


Fig. 7. Displacements for a  $[45/0]_{3S}$  beam

Table 1. AS4/3501-6 ply properties

$E_1$ (GPa)	142
$E_2$ (GPa)	9.8
$G_{12}$ (GPa)	6
$G_{23}$ (GPa)	3.45
$\nu_{12}$	0.3
$\nu_{23}$	0.43
$\rho$ ( $kg/m^3$ )	1580

Table 2. Bearingless Rotor characteristics

Number of blades, $N_b$	4
Radius, R (in)	36.0
Chord/Radius, $C/R$	0.0847
Thrust level, $C_w/\sigma$	0.08
Lift Coefficient, $C_l$	5.73
Drag Coefficient, $C_{d0}$	0.01
Solidity, $\sigma$	0.1079
Lock Number, $\gamma$	8.357
Blade Prepitch, $\theta_p$ (deg.)	4.0
Pitch Link Spring Stiffness, $K_p/m_0\Omega^2R$	58.606
Pitch Link Offset from Elastic Axis, $d/R$	0.03111

Figures 6 and 7 show the results of the present static analysis compared with the experimental and analytical results given in Ref. [7]. The material of composite rectangular beam is chosen as AS4/3501-6 graphite/epoxy and the ply properties are given in Table 1. Figure 6 show the static results of  $[0/90]_{3S}$  layup without any coupling, figure 7 show those of  $[45/0]_{3S}$  layup to illustrate the effect of bending-twisting coupling[7]. The length is 560 mm, the width is 30 mm and the ply thickness is 0.134 mm. The results show the axial( $u$ ), lead-lag( $v$ ), and flap( $w$ ) tip displacements for various layup beam under a tip vertical load, respectively. The agreement between the results of two analysis and experimental data is good. Aeroelastic analysis of bearingless rotors with composite rectangular flexbeam of two layup configuration, balanced layup  $[0_6/(\pm\theta)_3/(\pm45)_3]_S$  and unbalanced layup  $[0_6/-\theta_6/(\pm45)_3]_S$ , are performed using the large deflection beam theory

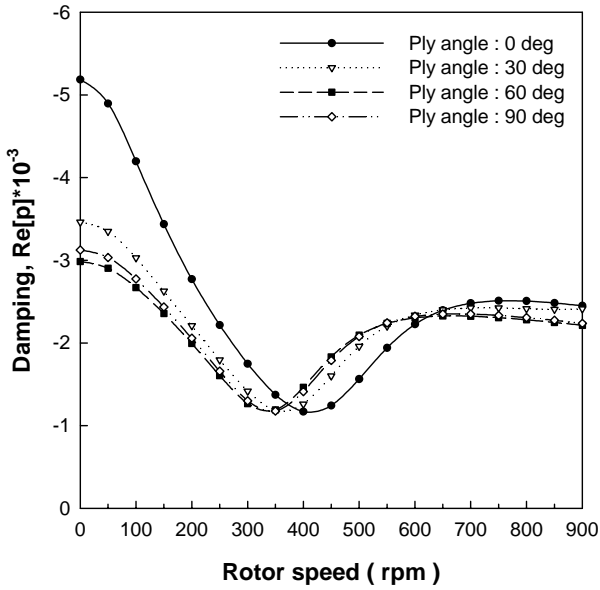


Fig. 8. Lag damping vs. rotor speed for balanced layup in hover

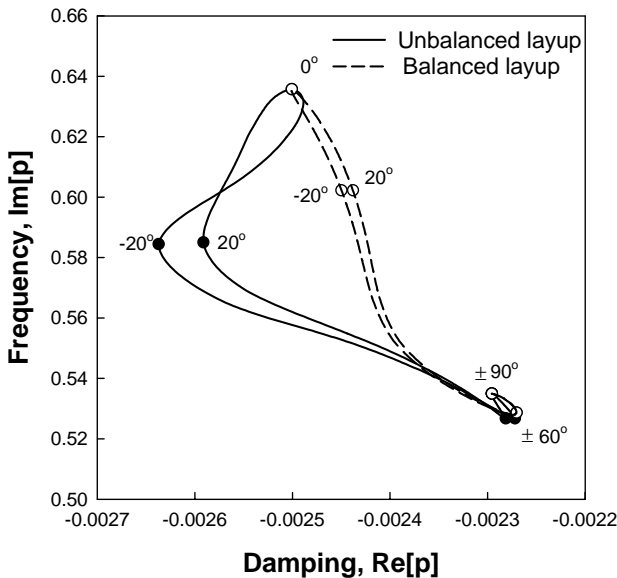


Fig. 9. Root locus plots for the lag mode for balanced and unbalanced layup in hover

in hover to investigate the effects of the structural couplings due to the ply orientation of the composites. The material properties of composite rectangular flexbeam for the present analysis are chosen as AS4/3501-6 graphite/ epoxy. The rotor characteristics used for numerical computation are presented in Table 2. Figure 8 shows that as the rotor speed is increased, the lag damping obtained in the present analysis is gradually decreased until 300~400 rpm but augmented from that at various ply angles for the balanced layup. Figure 9 shows

the root locus plots of complex eigenvalues vs ply angles for the first lead-lag mode about the two layup at 817 rpm. A positive ply angle relatively destabilizes the lag mode and a negative angle stabilizes the lag mode. The bending-twist structural coupling exists in the balanced and unbalanced layup and those of unbalanced layup are higher than those of balanced layup in some part of the ply orientation. Thus, the bending-twist structural coupling influences the stability of the lag mode. Figure 10 shows the flap and lag tip deflections of balanced layup for advanced ratio  $\mu = 0.2$ . An aspect of tip deflections is different as ply angles. Figure 11 shows the lag damping at various ply angles for the balanced layup as an advance ratio. Thus, the bending-twist structural coupling influences the tip deflections and the stability of the lag mode.

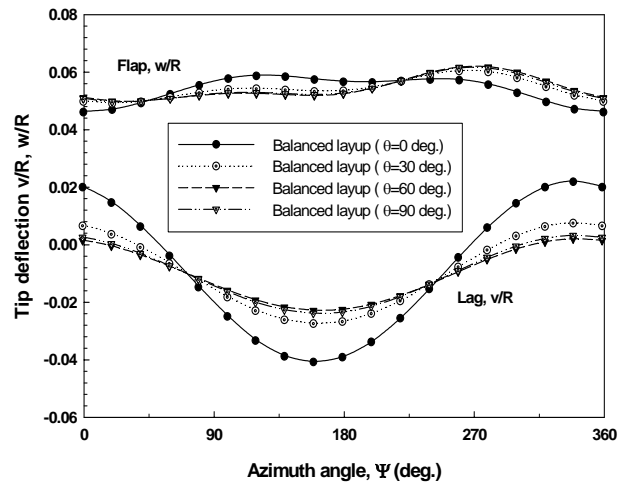


Fig. 10. Steady tip deflections in forward flight

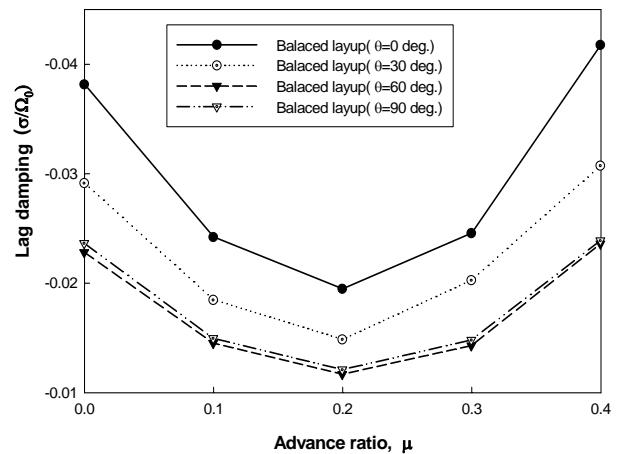


Fig. 11. First lag mode damping with different advance ratio

## 4 Conclusions

The aeroelastic stability of a bearingless rotor with composite flexbeam in hover and forward flight has been investigated. The cross-sectional constants of the composite flexbeam are obtained through two-dimensional analysis using a finite element method. The large deflection beam theory is used for the one-dimensional global analysis undergoing arbitrary large deflections and rotations. Numerical results of static analysis for the rectangular composite beams correlate very well with the previously published experimental results. The effects of the structural couplings on the stability of the bearingless rotors have been investigated for various ply configuration of the rectangular composite flexbeams. The stability of the lag mode is significantly influenced by the bending-twist coupling in hover and forward flight.

## Acknowledgments

This research has been supported by the KARI under KHP Dual-Use Component Development Program funded by the MOCIE.

## References

- [1] Friedmann, P.P., "Rotary-wing aeroelasticity: current status and future trends". *AIAA J.*, Vol. 42, No. 10, pp 1953-1972, 2004.
- [2] Rosen, A., and Friedmann, P.P., "The nonlinear behavior of elastic slender straight beams undergoing small strains and moderate rotations". *ASME Journal of Applied Mechanics*, Vol. 46, No. 1, pp 161-168, 1979.
- [3] Hodges, D.H., "A theoretical technique for analyzing aeroelastic stability of bearingless rotors". *AIAA J.*, Vol. 17, No. 4, pp 400-407, 1979.
- [4] Chopra, I., "Dynamic stability of a bearingless circulation control rotor blade in hover". *Journal of the American Helicopter Society*, Vol. 30, No. 4, pp 40-47, 1985.
- [5] Chopra, I., "Dynamic stability of a bearingless circulation control rotor blade in forward flight". *Journal of the American Helicopter Society*, Vol. 33, No. 3, pp 60-67, 1988.
- [6] Anita, L.T., and Chopra, I., "Aeroelastic analysis of a composite bearingless rotor in forward flight using an improved warping model". *Journal of the American Helicopter Society*, Vol. 40, No. 3, pp 80-91, 1995.
- [7] Minguet, P., and Dugundji, J. "Experimental and Analysis for Composite Blades Under Large Deflections Part 1: Static Behavior". *AIAA J.*, Vol. 28, No. 9, pp 1573-1579, 1990.
- [8] Atilgan, A.R., and Hodges, D.H. "Unified Nonlinear Analysis for Nonhomogeneous Anisotropic Beams with Closed Sections". *AIAA J.*, Vol. 29, No. 11, pp 1990-1999, 1991.
- [9] Cesnik, C.E.S., and Hodges, D.H., "VABS: a new concept for composite rotor blade cross-sectional modeling". *Journal of the American Helicopter Society*, Vol. 42, No. 1, pp 27-38, 1997.
- [10] Jeon, S.M., Cho, M.H., and Lee, I., "Static and dynamic analysis of composite box beams using large deflection theory". *Computers and Structures*, Vol. 57, No. 4, pp 635-642, 1995.
- [11] Cho, M.H., and Lee, I., "Aeroelastic stability of hingeless rotor blade in hover using large deflection theory". *AIAA J.*, Vol. 32, No. 7, pp 1472-1477, 1994.
- [12] Lim, I.G., and Lee, I., "Aeroelastic analysis of bearingless rotors using large deflection beam theory". *AIAA J.*, Vol. 45, No. 3, pp 599-606, 2007.